Geophysical Prospecting EAGE EUROPEAN ASSOCIATION OF GEOSCIENTISTS & ENGINEERS

Geophysical Prospecting, 2014, **62**, 658–674 doi: 10.1111/1365-2478.12104

Coil response inversion for very early time modelling of helicopter-borne time-domain electromagnetic data and mapping of near-surface geological layers

Cyril Schamper*, Esben Auken and Kurt Sørensen

Hydrogeophysics Group, Department of Geoscience, Aarhus University, Denmark

Received January 2012, revision accepted January 2013

ABSTRACT

Very early times in the order of 2–3 μs from the end of the turn-off ramp for time-domain electromagnetic systems are crucial for obtaining a detailed resolution of the near-surface geology in the depth interval 0–20 m. For transient electromagnetic systems working in the off time, an electric current is abruptly turned off in a large transmitter loop causing a secondary electromagnetic field to be generated by the eddy currents induced in the ground. Often, however, there is still a residual primary field generated by remaining slowly decaying currents in the transmitter loop. The decay disturbs or biases the earth response data at the very early times. These biased data must be culled, or some specific processing must be applied in order to compensate or remove the residual primary field. As the bias response can be attributed to decaying currents with its time constantly controlled by the geometry of the transmitter loop, we denote it the 'Coil Response'. The modelling of a helicopter-borne time-domain system by an equivalent electronic circuit shows that the time decay of the coil response remains identical whatever the position of the receiver loop, which is confirmed by field measurements. The modelling also shows that the coil response has a theoretical zero location and positioning the receiver coil at the zero location eliminates the coil response completely. However, spatial variations of the coil response around the zero location are not insignificant and even a few cm deformation of the carrier frame will introduce a small coil response. Here we present an approach for subtracting the coil response from the data by measuring it at high altitudes and then including an extra shift factor into the inversion scheme. The scheme is successfully applied to data from the SkyTEM system and enables the use of very early time gates, as early as 2–3 μs from the end of the ramp, or 5–6 μs from the beginning of the ramp. Applied to a large-scale airborne electromagnetic survey, the coil response compensation provides airborne electromagnetic methods with a hitherto unseen good resolution of shallow geological layers in the depth interval 0–20 m. This is proved by comparing results from the airborne electromagnetic survey to more than 100 km of Electrical Resistivity Tomography measured with 5 m electrode spacing.

Key words: Transient airborne, Early times, Near-surface.

*E-mail: cyril.schamper@geo.au.dk

INTRODUCTION

Airborne electromagnetic (AEM) methods with controlled sources are divided into two principal families: the frequency-domain and the time-domain (transient) systems. The time-domain systems are used intensively for groundwater and mineral exploration and in some cases provide an investigation depth of up to 500–800 m, while surface resolution is limited. In contrary the frequency-domain AEM systems are used for near-surface mapping because they have a content of higher frequencies (corresponding to early times), but they rarely reach a depth of investigation larger than 70–100 m even above resistive grounds (Siemon, Christiansen and Auken 2009). From the 1950s to the late 1980s, transient AEM systems were mainly fixed-wing systems where a transmitter loop was slung around an airplane and a receiver bird towed behind the aircraft. Not until the early 2000s did mature helicopter transient AEM (HTEM) systems appear (Allard 2007). With helicopter AEM systems it is easier to control the flight speed and to fly at low altitudes in order to obtain an optimal resolution of the more shallow geological layers.

To achieve a similar near-surface resolution for time-domain systems compared to frequency-domain systems, it is necessary to measure data right after the turn-off of the current in the transmitter loop. This corresponds to achieving high frequencies (Nyboe and Sørensen 2012). Steuer, Siemon and Auken (2009) presented a comparison of groundwater data acquired by a DIGHEM system with a highest frequency of 192 kHz and a SkyTEM system with a first gate around 17 μs. Seventeen μs is relatively late and the HTEM system failed to provide a similar near-surface resolution in the upper 20 m as obtained from the HFEM system. To improve the near-surface resolution, it is necessary to consider the earth response immediately after the turn-off of the transmitter current, i.e., the first 5–20 μs depending on the system. However, these data are often disturbed by a systematic primary response caused by an exponentially decaying current in the transmitter loop; hence we name it the Coil Response (CR). The CR is caused by small currents often less than 0.01 A. The CR is more critical for AEM systems compared to ground-based TEM systems, because the measured secondary fields from the ground decay with increasing flight altitude and, as importantly, the receiver coil is physically located much closer to the transmitter wires.

The method presented for handling CR was first reported in an abstract by Auken, Foged and Sørensen (2010) and after obtaining a few years' experience with field data it is now the subject of this paper. Another CR handling technique applied to the helicopter-borne AEM system VTEM was presented in an abstract by Macnae and Baron-Hay (2010) and applied to a survey with a newly designed VTEM system by Legault *et al*. (2012). It has to be noted that the two approaches are fundamentally different and have been developed independently. While the source waveform in our forward modelling algorithm is fully modelled as it is measured, it is deconvolved in the Macnae and Baron-Hay (2010) approach to get the response due to a step-off or a perfect linear ramp prior to the inversion. Macnae and Baron-Hay (2010) identified that this deconvolution was not sufficient to obtain reliable early-time data before 100 μs and that a constant 'parasitic' response with a linear phase response (i.e., an exponential decay with a certain time relaxation constant) was still present after the deconvolution. The parasitic response is the CR in our definition. They also found that the amplitude and the sign of the parasitic response vary. Thanks to the convolution of the exponential decay of the parasitic response determined from high-altitude measurements with the received primary field, Macnae and Baron-Hay (2010) succeeded to obtain usable time gates down to 10–20 μs after the end of the ramp. In the present paper we push this limit down to 2–3 μs after the turn-off.

In this paper, the CR shape is monitored during high-altitude (HA) measurements and then modelled simultaneously with the ground response induced by the true waveform during the inversion of the data. A supplementary parameter has been added to correct for the amplitude variations of the CR caused by small deformations of the centimetre size of the carrying frame, occurring when the frame moves in the air space. By this we obtain very early time gates, only a few μs after the end of the ramp-off, meaning that the limit of what can be obtained from off-time measurements is reached.

We first reprise the theory from Kamenetsky and Oelsner (2000) explaining the origin of the CR for an AEM system. The theory is then confirmed by field measurements at HA with the SkyTEM system (Fig. 1). Then the procedure for modelling the CR during the inversion is detailed and finally applied to an entire survey to illustrate the effect of CR modelling on the near-surface resistivity distribution. We use a survey of about 100 km of ERT data to confirm the AEM resolution of the shallow geology in the top 20 m.

ORIGIN OF THE COIL RESPONSE FROM THEORETICAL INSIGHTS

Equivalent electronic circuit of the transmitter wire

Kamenetsky and Oelsner (2000) presented an analysis of distortions during early times for a ground TEM device in the

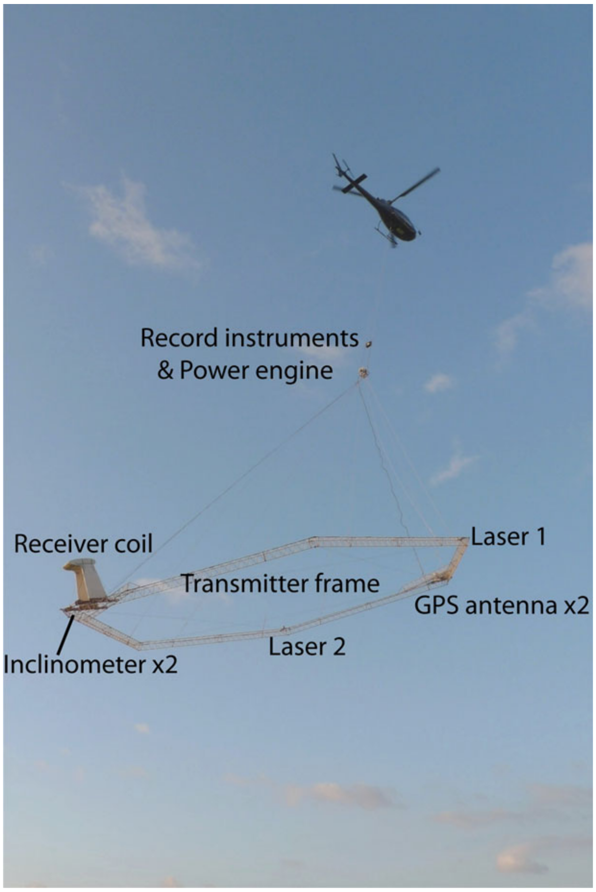

Figure 1 The SkyTEM system, here with a transmitter loop of 314 m^2 (SkyTEM304). All flight systems, GPS, inclinometers, lasers are doubled to ensure continuous monitoring of the system.

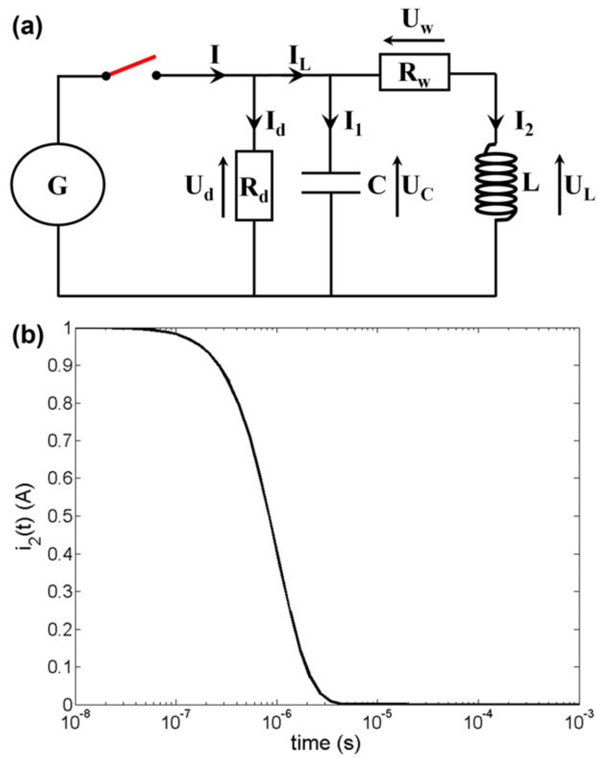

Figure 2 Coil Response of the transmitter loop explained by an equivalent circuit. (a) Equivalent electronic circuit of the transmitter loop. (b) Decay of the current in the transmitter loop after a step-off at $t = 0$ s (cf. equation (1)) for an initial current of 1A and a loop size of 40 m x 40 m.

coincident loop configuration (same loop for transmission and reception). Following their work, the transmitter loop of the transient AEM is modelled by an equivalent electronic circuit as shown in Fig. 2(a). The generator, G, injects current into the circuit where the self-inductance of the loop, L, is related to the dimensions and to the number of turns of the wire. The resistance, R_d, is the damping resistance, R_w is the resistance of the transmitter wire and the capacitor, C, represents the capacitance of the loop.

In this paper we deal with a receiver loop separated from the transmitter loop (Fig. 1) and the most interesting part of the circuit of Fig. 2(a) is I_2, which is the current circulating in the transmitter wire. With this current described, it is possible to deduce the self-response of the system measured in the receiver loop.

As Kamenetsky and Oelsner (2000) showed, the current in the transmitter wire for a step-off of drive current I can be expressed in the time domain as (cf. demonstration in the Appendix):

$$i_2(t) = I\,(1 + at)\,\mathrm{e}^{-at}, \qquad (1)$$

with $a = 1/\sqrt{LC}$.

Note that the low resistance of the wire R_w has been considered as negligible so that only the inductance L and the capacitance C of the transmitter wire have been kept (see demonstration in the Appendix). Furthermore, Kamenetsky and Oelsner (2000) suggested that the inductance measured in Henry of a square loop of side length s can be estimated by $L \approx 5\mu_0 s \approx 0.625 \times 10^{-5} s$ with μ_0 being the magnetic permeability of free space. In this paper we use the expression provided by Grower (1946), which gives similar values:

$$L[\mu\mathrm{H}] \approx s(0.8\ln(s/r_w) - 0.41), \qquad (2)$$

where r_w is the radius of the wire in metres.

Equation (2) gives an inductance of $L \approx 150\mu H$ for a square loop with a side length of 20 m and a wire diameter of 2 mm. Since the focus of this paper is on the very early times for which low injected current is used, the transmitter wire employed is generally thin.

Also the capacitance can be estimated as:

$$C \approx C_{dl}/4s, \tag{3}$$

where C_{dl} is the linear capacitance of the wire and $1/C = \int_0^{4s} \frac{1}{C_{dl}} dl$.

For a copper wire of about 2 mm diameter the linear capacitance $C_{dl} \approx 160 \times 10^{-9}$F/m (Timofeev and Novikov 1990), which gives a total capacitance $C = 2 \times 10^{-9}$F for a square loop of s x $s = 20$ m x 20 m. Considering an injected current $I = 1\,A$, these numbers give the decrease of the current in the transmitter loop that steps-off instantly at time zero. Equation (1) predicts a decay of loop current as in Fig. 2(b). As expected, the decay loop current is not a perfect step-off, it actually lasts several μs. This shape of the ramp-off has to be modelled and taken into account in the forward modelling to avoid biased estimation of the very early time gates during the inversion, like other critical system parameters such as flight altitude, or low-pass filters (Christiansen, Auken and Viezzoli 2011).

Coil response measured at receiver coil position

The source waveform is accurately modelled with several successive linear ramps following the seminal work from Fitterman and Anderson (1987). The amplitude of the waveform is set to zero at a defined turn-off time, which usually corresponds to the time where the accuracy of the amplitude monitoring is reached, i.e., ~ 0.01 A or about 3 μs after the beginning of the turn-off ramp for the SkyTEM configuration we are working with in this paper. All gates after this defined turn-off time are considered as off-time gates and the residual primary field – the CR – coming from the small amount of remaining current is identified as contamination and not modelled with the waveform. It has to be underlined that the zero timing defined in this paper always corresponds to the beginning of the ramp-off and not to the end of the waveform unless otherwise specified; for obvious reasons it is a badly determined point from a modelling perspective.

As the CR considered after the turn-off time corresponds to a residual current at least one hundred times lower than the total injected current, the in-phase secondary (or inductive) response from the ground, which is caused by the CR current, can be considered as negligible compared to the out-of-phase secondary field induced by the essential part of the source waveform. Therefore only the primary CR is modelled and the CR will always refer to the primary component. Starting from the well-known Biot-Savart law, which gives the induction field generated by a current going through a wire:

$$\boldsymbol{b}(t) = \frac{\mu_0}{4\pi} \int_C \frac{i_2(t)\boldsymbol{dl} \times \boldsymbol{r}}{|\boldsymbol{r}|^3}, \tag{4}$$

where $\boldsymbol{b}(t)$ is the primary induction field generated by the wire with the contour C, $i_2(t)$ the current going through the wire, $\boldsymbol{dl}$ the infinitesimal vector belonging to the wire and $\boldsymbol{r}$ the vector from the position of the infinitesimal wire to the point of observation.

Equation (4) can be simplified for an x-oriented unit electric dipole $\boldsymbol{dl} = (dx, 0, 0)$, which gives for the vertical component of the electromotive force:

$$\frac{\partial b_z}{\partial t}(t) = \mu_0 \frac{i_2'(t) dx \Delta y}{4\pi r^3}, \tag{5}$$

where Δy corresponds to the distance between the unit electric dipole and the receiver position in the y- direction.

One can observe from equation (5) that the time decay of the CR only depends on $i_2'(t)$. This means that if $i_2'(t)$ remains identical, it ensures that the CR time decay remains unchanged as also confirmed with field measurements shown in the next part of the present paper, and that only the CR amplitude is affected by a factor due to a change in the position of the receiver coil. This observation is for a unit electric dipole but the spatial factor of equation (5), i.e., $\mu_0 dx \Delta y/(4\pi r^3)$, can easily be integrated numerically along the perimeter of the transmitter loop to estimate what can be called the amplitude factor of the CR. Note that this factor can be positive or negative depending on the position. The result of this integration is shown in Fig. 3(a) considering the loop geometry of the SkyTEM system of 314 m^2. The receiver loop height, relative to the transmitter plane, is fixed to 2.1 m, so the amplitude of the primary field is shown in the (x,y)-plane. The spatial factor of equation (5) is quite homogeneous inside the transmitter loop where it reaches its maximum. One can see a narrow white ring located slightly outside of the transmitter wire, the position of which is represented by a green dashed line. This white ring corresponds to a change of sign of the primary field, crossing zero. Figure 3(b) shows the amplitude factor of the CR along the profile, drawn as a black line in Fig. 3(a). In the SkyTEM system, the receiver position is chosen so that it is located as close as possible to the 'white' ring. This is in order to obtain the lowest CR possible, i.e., to get the CR negligible compared to the ground response.

As illustrated in Fig. 3(b), the CR amplitude factor changes its sign within a very short distance. This implies careful fine-tuning of the receiver loop positioning before

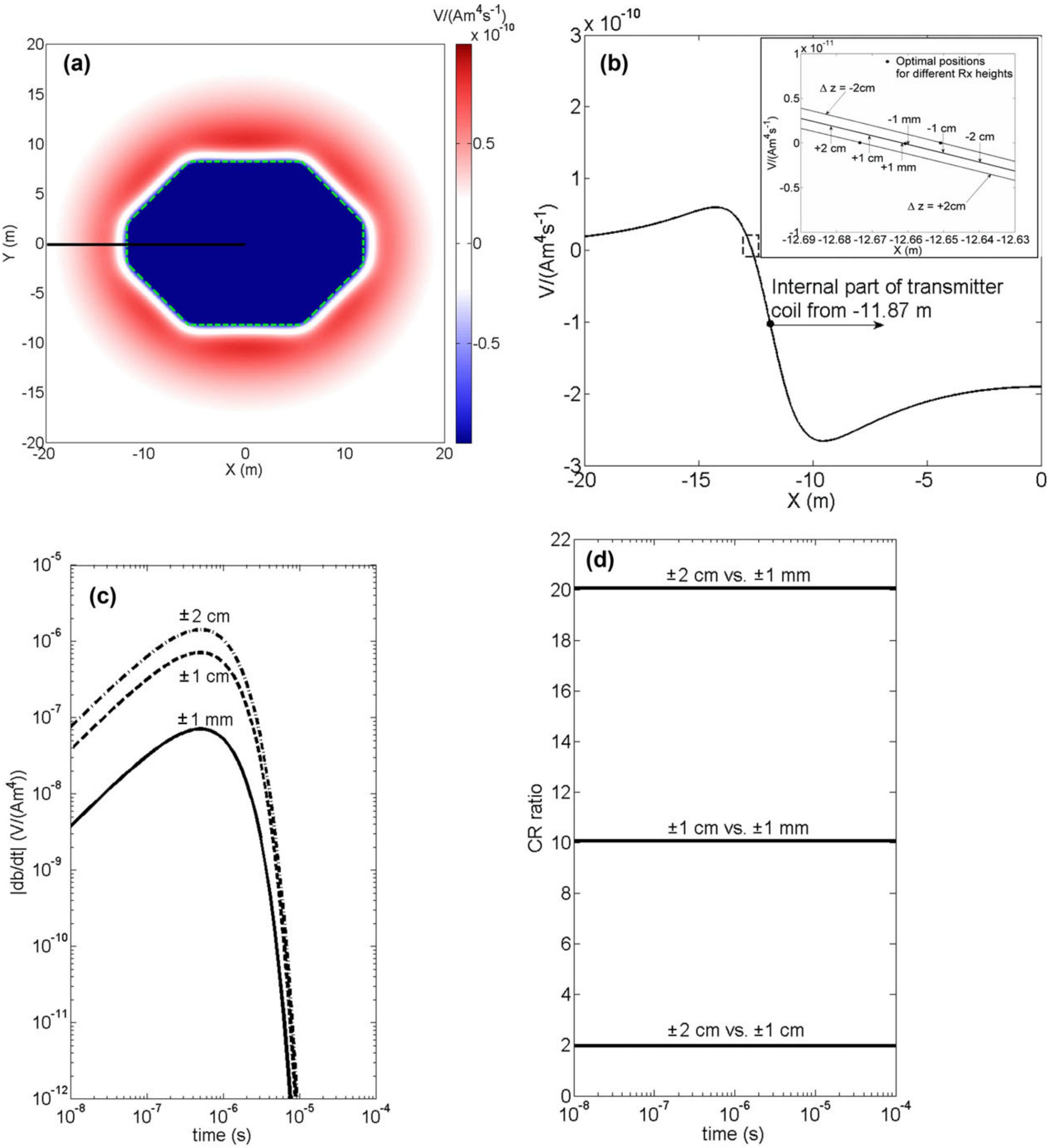

Figure 3 Coil Response generated by the remaining small current in the transmitter loop. (a) Normalized amplitude factor of the CR around the SkyTEM loop. The dashed green line indicates the loop frame and the solid line the profile shown in (b); (b) normalized amplitude factor of the CR along the x-axis (flight direction); (c) the CR measured at different lateral positions along the x-axis, the optimal one corresponds to the minimum in (b) with a precision of less than 1 mm; (d) ratio of the measured CR at different lateral positions compared to the optimal one.

initiating a survey. Let us now consider all elements of equation (5) by including the derivative of the injected current $i_2'(t)$, which allows us to simulate the CR measured at the receiver coil in Fig. 3(c). The modelling is made for an inaccurate positioning of the coil of $\pm$ 1mm, $\pm$ 1cm and $\pm$ 2 cm around the optimal position where the CR is theoretically null. A maximum of a few cm deformations has been considered according only to observations made on the field with SkyTEM equipment. The curves in Fig. 3(c) show that the CR is decreasing quickly after 1–2 μs and positive and negative lateral shifts induce almost the same change in the amplitude of the CR, despite the opposite sign (Fig. 3b).

The effect of a vertical displacement of the receiver coil is illustrated in the inset of Fig. 3(b) for a Δz of +2 cm and -2 cm. Such a vertical move induces a shift of the optimal position by the same range, i.e., a few cm. A vertical displacement implies a similar change in amplitude as a lateral displacement in the x-direction.

The behaviour for a displacement in the y-direction, i.e., perpendicular to the flight direction, can be deduced by looking at the isolines of Fig. 3(a). Along the x-axis going through the centre of the transmitter loop, the tangents of the isolines are perpendicular to the x-axis, i.e., y oriented. A movement of the receiver coil in the y-direction will then induce a limited change in the amplitude of the CR compared to a shift in the x-direction.

The differences compared to the optimal position are displayed as ratios in Fig. 3(d) and show that the time decay of the CR is constant but shifted by a given factor as anticipated by equation (4) for a unit electric dipole.

Finally, Fig. 4 compares the CR to the ground response of a homogeneous earth of 100 Ωm whose response is measured at altitudes of 30 m and 50 m. One observes that the final slope of the CR is much steeper than the one from the earth response decreasing proportionally to -5/2 in log-log space. The ground response contaminated by the CR remains very close to the uncontaminated one (black curve) if the receiver coil is located at the optimal position (still with a precision of less than 1 mm), or laterally shifted by ± 1 cm. The effect on the first three gates at 5.2, 6.2 and 7.2 μs is clearly visible when the position shift reaches ± 10 cm. An intermediate shift of a few cm will be located in-between. Figure 4 also illustrates the fact that the impact of the CR is less important when the flight altitude is lower, i.e., when the earth response is stronger.

COIL RESPONSE MEASURED AT HIGH ALTITUDE

The SkyTEM system (Fig. 1) was developed in Denmark and has steadily improved over the last 10 years (Sørensen and Auken 2004). It is a helicopter transient electromagnetic system, which has been specially designed for groundwater mapping but is now also used for mineral exploration. During the last two years the very early times before 12 μs have been used regularly for interpretation of production data for groundwater exploration (Auken *et al.* 2010). With the last version of the SkyTEM system, the Mini-SkyTEM (SkyTEM101), the first gate used after the beginning of the ramp-off is at 5–6 μs (Schamper, Auken and Sørensen 2012).

To model the effect of the CR, we first need to measure it at high altitude (> 400 m) where the earth response is below the noise level. A sounding curve measured at 1000 m is displayed in Fig. 5(a). This curve represents a stack of several minutes and allows computation of the standard deviation at each gate. It shows that the measured CR is repeatable until 7–8 μs where the noise floor is reached due to the absence of the ground response. In this case the CR is lower than the sounding curves recorded at altitudes of 30 m and 55 m (Fig. 5a). At 30 m the ground response is almost one decade above the CR before 10 μs, whereas the 55 m curve is of the same order. These low altitude sounding curves were measured in an area where the resistivity of the first 20 m is close to or below 100 Ωm, so it is important to note that the ground response would have been lower and closer to the CR level, even at 30 m, for a more resistive subsurface.

Figure 5(b) shows the measurements of the CR at high altitude taken at the beginning of a survey and after a week of surveying. In order to compare the time decay of the CR at these two moments, the CR measurement at the end of the survey is normalized so that the value at the first gate is the same as the one of the first recorded CR. The two curves are on top of each other, which confirms that the time decay of the CR remains identical and that only the magnitude has to be determined. For this we designed a special inversion procedure.

INVERSION WITH MODELLING OF THE COIL RESPONSE AT PRODUCTION ALTITUDE

Previous theoretical developments and field measurements of the CR have led to the following conclusions:

- The residual primary field at high altitude clearly has the same characteristics as the CR modelled from theoretical circuit analysis, which supports the explanation of field measurements at very early times
- CR modelling allows the definition of an optimal position for the receiver coil so that the CR is as low as possible compared to the ground response.

As the CR has been clearly explained and identified in the data, it is now possible to compensate for the CR when interpreting early times. As shown, the CR has a stable shape but has amplitude changes. This means that we cannot

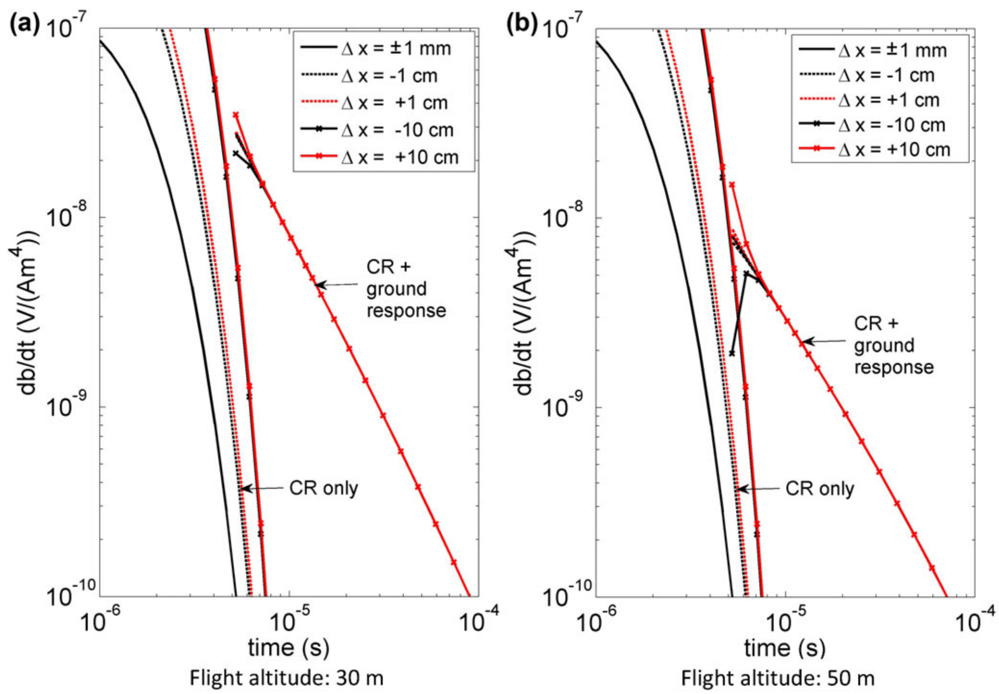

Figure 4 Earth response of a half-space of 100 Ωm measured at an altitude of 30 m (a) and 50 m (b). The ground response is disturbed by the different CRs shown in Fig. 3(c). Here only a lateral shift of ± 10 cm of the receiver coil shows a clear impact on gates before 10 μs at both altitudes. The turn-off time considered is 3.3 μs and the first gate measured located at 5.2 μs; the next three gates are at 6.2 μs, 7.2 μs and 8.2 μs.

subtract it directly from the measurements. Instead, we propose to fix the CR shape and then invert for a scaling factor that will correct for the amplitude variations. The scaling factor is then a supplementary parameter in the regularization problem (Auken and Christiansen 2004) where resistivities, depths and flight altitudes are inverted. Field tests have shown that as the CR changes slowly during a flight, the CR scaling factor should be tightly constrained in the flying direction to impose only very slow variations. In this case we use the spatially constrained inversion (SCI). A new description of the SCI inversion scheme is outside the scope of this paper and we therefore refer to Viezzoli *et al.* (2008). The SCI scheme in this paper is designed so the CR factor is only constrained along the flight lines and not between the lines.

Figure 6 illustrates how the consideration of this CR scaling factor improves the fit of the earliest gates. Figure 6(a) illustrates the SkyTEM sounding with both low-moment (LM) and high-moment (HM) curves. To better see the fit at the early gates, zooms on the LM curves are shown in Fig. 6(c,d) when the CR is not considered or modelled, respectively. As seen in Fig. 6(c) with the CR not considered, the fit of the early gates is far from perfect, which is not the case in Fig. 6(d) where the CR is modelled and the scaling factor estimated. The data residual of the sounding is consequently lower and drops from 1.19 to 0.84. Figure 6(b) shows the resistivity models estimated for the two inversions (both are smooth inversions with 20 layers where only resistivities are inverted) with noticeable changes in the upper 30 m with the CR considered.

APPLICATION TO AN AIRBORNE ELECTROMAGNETIC SURVEY (SORØ, DENMARK)

To illustrate the resolution capabilities when considering the CR, we show results from a SkyTEM survey flown in 2009 in the Sorø region, Denmark (Fig. 7). The geological description of the area is detailed in Fig. 8 (from Rapport Naturstyrelsen 2008). The geological context is sedimentary with first a succession of sub-horizontal layers of Quaternary glacial sands and tills. Up to four different glacial sandy sediments can be identified for this period (Fig. 8a). They correspond to four different aquifers whose thicknesses and depths vary quite a lot across the area (Fig. 8b). Glacial tills are characterized by lower resistivity (20–40 Ωm) compared to the sand lenses (50–100 Ωm and above). These protecting clay layers

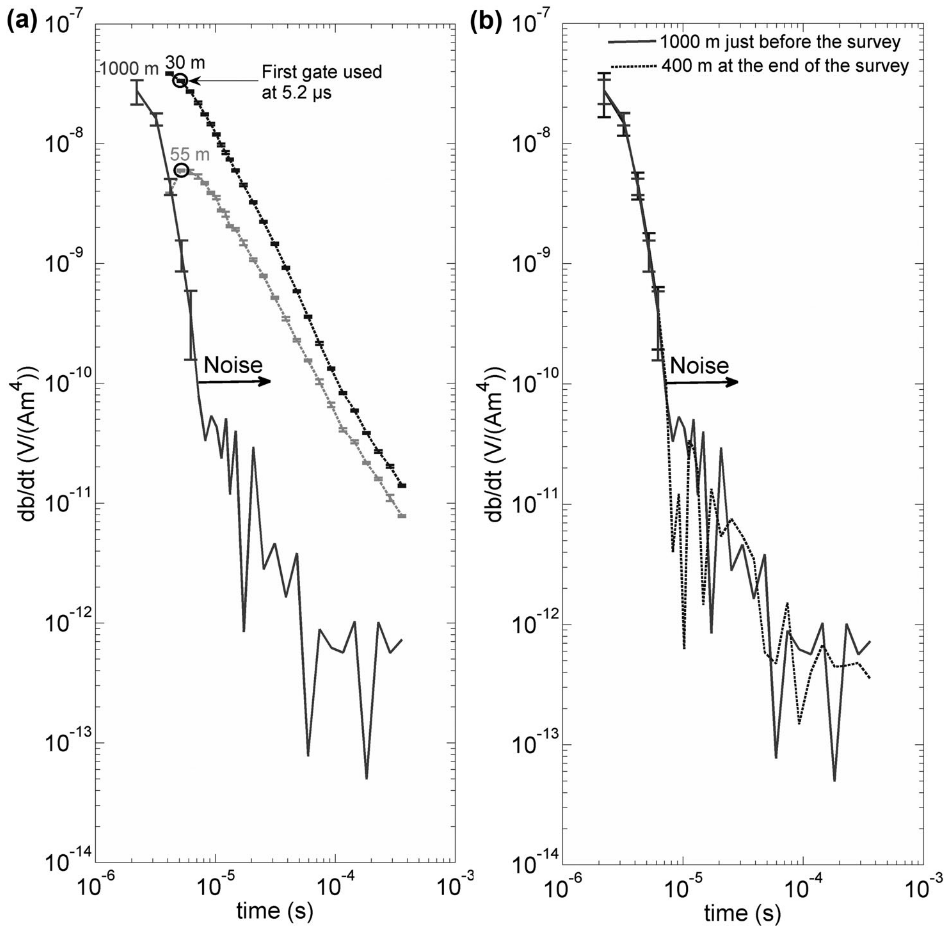

Figure 5 db/dt curves of the Super-Low-Moment (SLM) from the SkyTEM system: (a) measurement at an altitude of 1000 m contains only the coil response (CR), whereas the 30 m and 50 m curves contain both the CR and earth response; (b) high-altitude Coil Response (CR) at the beginning and at the end of the survey (the last CR is normalized so that the value at the first gate is equal to the one of the first CR). From the gate at 7.8 μs the measurements at high altitude are below the noise level and show erratic oscillations.

are expected to be well mapped with transient AEM thanks to their low resistivity. Just below the Quaternary layers, the pre-Quaternary Kerteminde marl with resistivity ranging from 10–20 Ωm can be found. The second deepest layer is a very conductive formation (< 5 Ωm), the green Lellinge sand-lime, which is saturated with residual saltwater. The deepest layer is the Danien chalk with a thickness exceeding 200 m. This last layer is not expected to be mapped below the two upper conductive pre-Quaternary formations.

The purpose of the survey was twofold: 1) to build a geological model of the area for groundwater flow modelling and evaluation of the groundwater resources; 2) to estimate the thickness of a shallow clay layer protecting underlying groundwater resources against pollution from intensive farming. The latter is normally performed by intensive use of electrical resistivity tomography (ERT) (Casas *et al.* 2008) as EM methods do not have sufficient resolution in the upper 10–15 m. As we will show, by correcting for the CR this can be done as well by SkyTEM measurement.

The survey consists in 900 km of flight lines flown with a transmitter loop of 314 m^2. Two transmitter moments are used, employing different current levels and a different number of turns. The low moment LM (8 A, 1 turn) with a very short turn-off time of 3.8 μs provides early times with near-surface information, whereas the high moment HM (93 A, 2 turns) allows for deeper information at later times (with a turn-off time of 26.7 μs).

The ERTs in the area constitute a total of about 100 km of profile lines. They were measured with the ABEM SAS 4000 Terrameter with an electrode spacing of 5 m and a gradient array, giving information from 1–2 m to approximately 40 m below the surface.

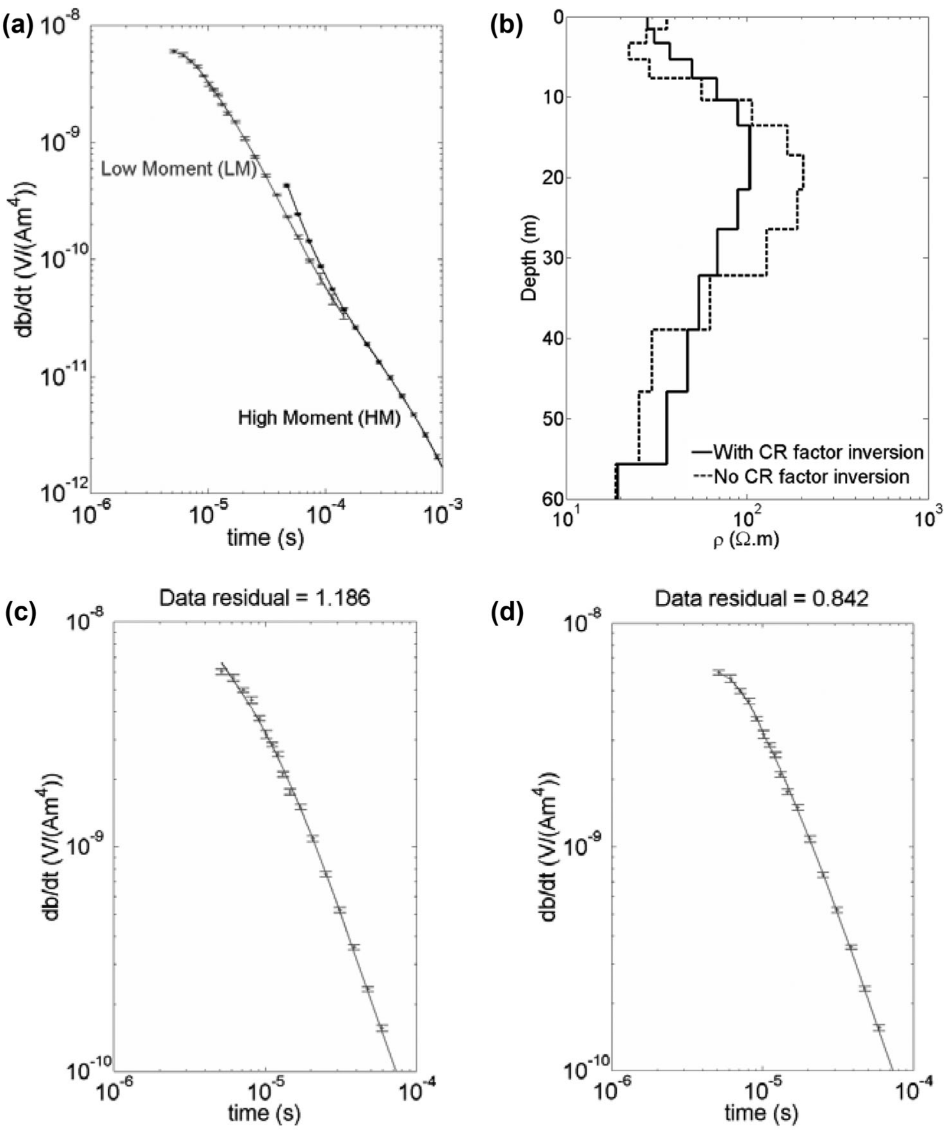

Figure 6 Inversion of a single sounding with or without the consideration of the CR factor: (a) typical SkyTEM sounding curve with both moments and the corresponding inversion result (solid line) without considering the CR; (b) smooth resistivity models obtained by considering or not considering the CR; (c) LM curve with the corresponding inversion result without considering the CR; (d) LM curve with the corresponding inversion result by considering the CR.

A laterally constrained inversion (LCI) (Auken and Christiansen 2004) is applied on a section of one of the flight lines (red line in Fig. 7) where ERT had been carried out (results of the inversion in Fig. 8(a) at a distance less than 50 m from the SkyTEM line). In the ERT section of Fig. 9(a) one sees four layers along the profile: a resistive first layer of 5–7 m with resistivity above 50 Ωm ($\geq$ 100 Ωm in the northern part of the profile), a conductive second layer of 10–15 m with resistivity around 30–50 Ωm, a resistive third layer of about 40 m with resistivity often above 100 Ωm and finally a conductive layer with resistivity below 30 Ωm. The top of this conductive last layer almost corresponds to the depth of investigation (DOI) of the ERT measurements, which is indicated by the transition to the shaded colours (Christiansen and Auken 2012). The resistivity as well as the depth to the top of the layer is better resolved with SkyTEM showing resistivity around 10–20 Ωm, indicating the presence of a clay layer (Fig. 10b–d).

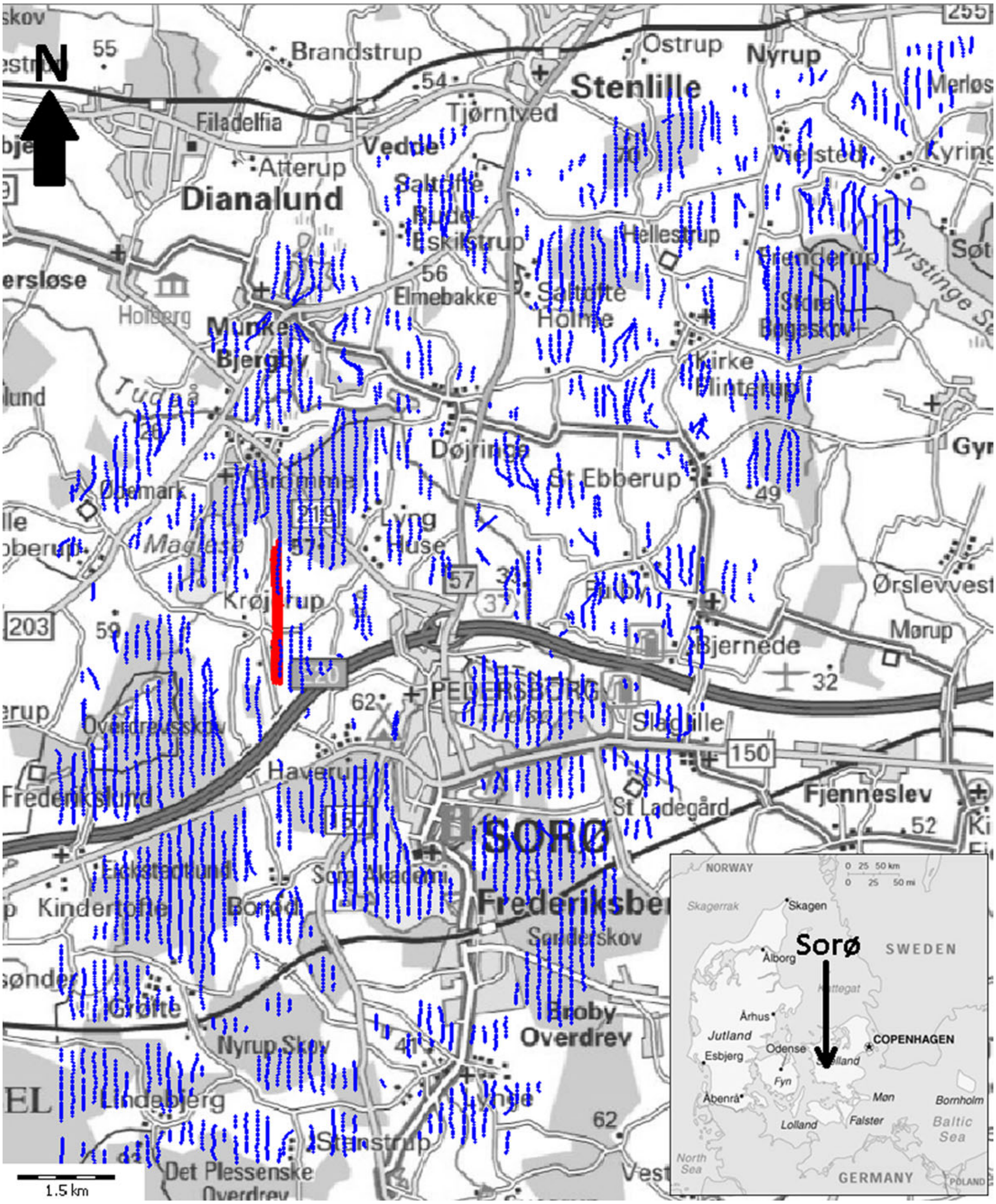

Figure 7 Survey flights (blue lines) above the Sorø survey area after processing and removing the disturbed data due to power lines. The thick red line above one of the flight lines corresponds to the section displayed in Fig. 9. The survey has 900 km of flight lines and is flown with a 314 m^2 frame, with both LM and HM moments.

The first SkyTEM section in Fig. 9b is the inversion result without consideration of the very early gates before 9 μs. In this case the CR can be neglected as its level is several decades below the earth response for all gates (Fig. 5a). The resistivity section for this case (Fig. 9b) is quite similar to the ERT one (Fig. 9a), especially in the south part of the profile where the resistivity of the first layer is in the medium-range (compared to the northern part) and its

(a)

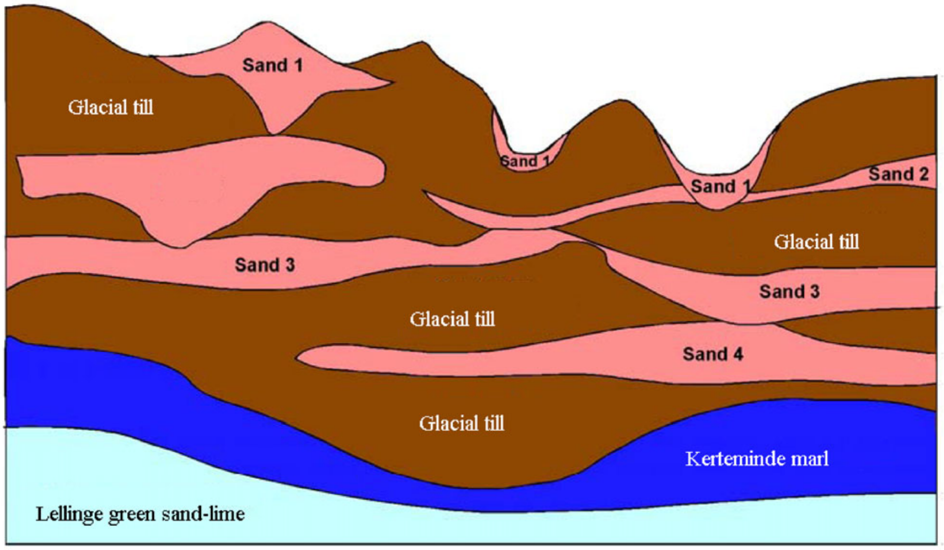

(b)

Age	Geology	Thickness (m)	Resistivity (Ωm)
Quaternary	Glacial sands & tills	Total thickness of 40-130	20-40 for tills 50 to >100 for sands
Pre-Quaternary	Kerteminde marl	< 10 to >100	10-20
	Lellinge green sand-lime	25 to >100	< 5 (residual saline water)
	Danien chalk	>200	-

Figure 8 Geology of the Sorø survey area: (a) conceptual scheme of the geology; (b) thicknesses and resistivity ranges of the different layers.

thickness larger. In the northern part the resistive layer is thinner (according to the ERT in Fig. 9(a)) and there is no longer sensitivity in the data to see it. Figure 9(c) shows the results for the same inversion setup but here four supplementary early gates before 9 μs are considered without CR correction. One observes that the resistivity contrast between the first two layers is much more pronounced compared to Fig. 9(b). The first resistive layer is thin and clearly above 100 Ωm everywhere, including in the south part of the profile. The second conductive layer is also thinner and more conductive compared to Fig. 9(a,b). This near-surface section seems unlikely according to the ERT in Fig. 9(a). If the CR correction is considered with the inversion of the shift factor (Fig. 9d), the resistivity section becomes close to what is obtained by ERT. Even between 200–550 m, the first layer appears clearly and is closer to the ERT compared to Fig. 9(b) where the layer is less pronounced. This finer vertical resolution of the near-surface is clearly provided by the four supplementary early gates and the CR correction.

Figure 9(e) illustrates the evolution of the estimated CR factor along the profile with its corresponding STD factor, which indicates how well the parameter is determined by the inversion. A value equal to 1 for the STD factor would mean that the parameter is perfectly determined. On the present plot the STD factor is close to 1 and the CR factor between 1–2 with a higher flight altitude (green line), i.e., above 40 m. Below this altitude the uncertainty on the CR factor is much larger (with a STD factor close to 2), which is related to the lower relative effect of the CR on the earth response at lower altitudes, as illustrated before in Fig. 5(a).

The example clearly shows that CR correction makes it possible to use gates as early as 5–6 μs or 2–3 μs from the end of the ramp, thereby giving sufficient resolution of very shallow geological layers. If the CR is not considered, the affected gates have to be culled in order not to obtain false images of the shallow geological layers. By this, one also obtains a worse resolution.

To mimic a quasi-3D distribution of the ground resistivity, a Spatially Constrained Inversion (SCI) is undertaken over the entire survey area. In the SCI lateral constraints are not only applied along the flight lines but also between neighbouring lines (Viezzoli *et al.* 2008). The SCI results are shown as

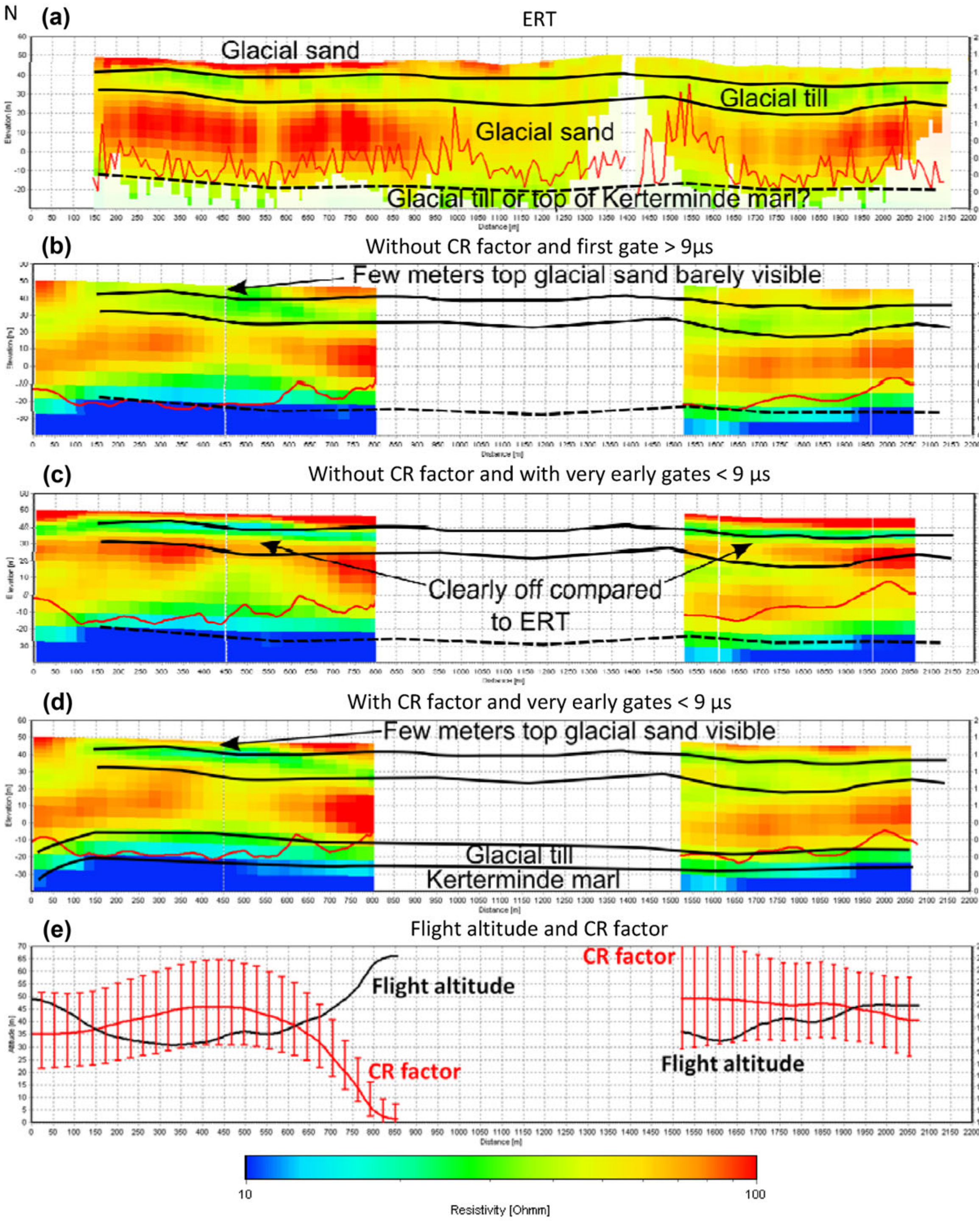

Figure 9 Resistivity sections: (a) ERT measurements with geological interpretation (from the geological model of Fig. 8), (b) inversion of SkyTEM data without CR factor inversion and very early gates, (c) inversion of SkyTEM data without CR factor inversion but with very early gates being considered, (d) inversion of SkyTEM data with CR factor inversion and very early gates, (e) flight altitude and CR factor. The blanked colours visible in (a) correspond to layers located below the depth of investigation (DOI), the ones for the SkyTEM sections (b–d) are not visible because the DOI is larger for the SkyTEM system compared to the ERT. The four additional gates considered before 9 μs are located at 5.8, 6.8, 7.8 and 8.8 μs with a turn-off ramp ending at 3.8 μs.

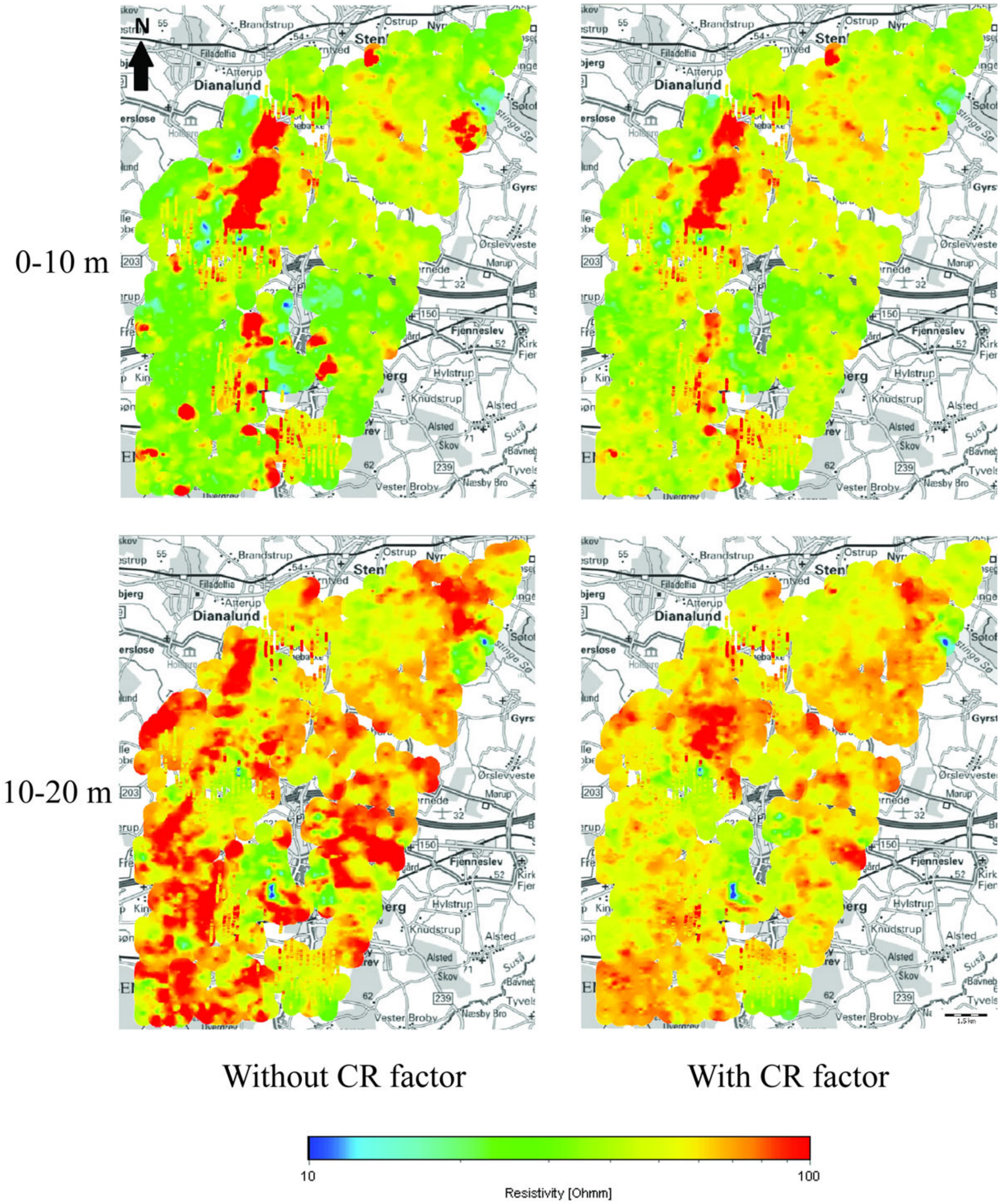

Figure 10 Mean resistivity maps of the nearsurface at two different depth intervals, with or without the inversion of the CR factor. Coloured points correspond to resistivity values obtained from ERT.

mean resistivity maps in Fig. 10, which provide an overview of the effect of CR for the two depth slices 0–10 m and 10–20 m. ERT resistivity values are superimposed with coloured points for comparison. Almost 100 km of ERT data were measured within the SkyTEM survey area. For the depth slice 0–10 m the inclusion of the CR increases the resistivity values, which become much closer to values observed with ERT. As pinpointed for the profile shown in Fig. 9(c), the resistivity contrast between the second layer and the surrounding ones is more pronounced when the CR is not considered. This is also observed when comparing the resistivity maps for the depth slice 10–20 m. The resistivity changes at this depth interval look more pronounced compared to the slice 0–10 m. This can be explained by the fact that the resistivity values at 10–20 m are higher, which makes this interval more sensitive to slight changes in the early times. Deeper resistivity maps are not shown here, but as suggested by the section in Fig. 9, the effect of the consideration of the CR has almost no effect below a depth of 30 m, which is also the approximate depth that can be determined from the resistivity models shown in Fig. 6(b).

Figure 11 shows the cross-plots between the mean resistivity determined from SkyTEM and the one coming from ERT. The same depth slices, i.e., 0–10 m (Fig. 11a) and 10–20 m (Fig. 11b), are considered as for Fig. 10. The considered SkyTEM resistivities are taken from soundings located less than 20 m from the ERT profiles. The correlation coefficients are calculated using the conductivity as it is expected that variations in high resistivity values are less determined by TEM measurements compared to DC. This can in fact be observed when looking at the highest resistivities (> 200 Ωm) as they tend to flatten, indicating that TEM has difficulty to resolve these high values.

All plots of Fig. 11 show that the cloud of blue points is more spread when the CR is not considered compared to when it is. This is shown with the black points. This visual observation is confirmed by the estimated correlation coefficients, which are higher for both depth intervals when the values are CR corrected. The improvement in the correlation with ERT resistivities is worse for the depth interval of 0–10 m, which can be due to short wavelength near-surface variations and to the different sensitivity footprints of the two geophysical methods. Despite those improvements at different levels, the overall benefit of the CR modelling is clearly demonstrated.

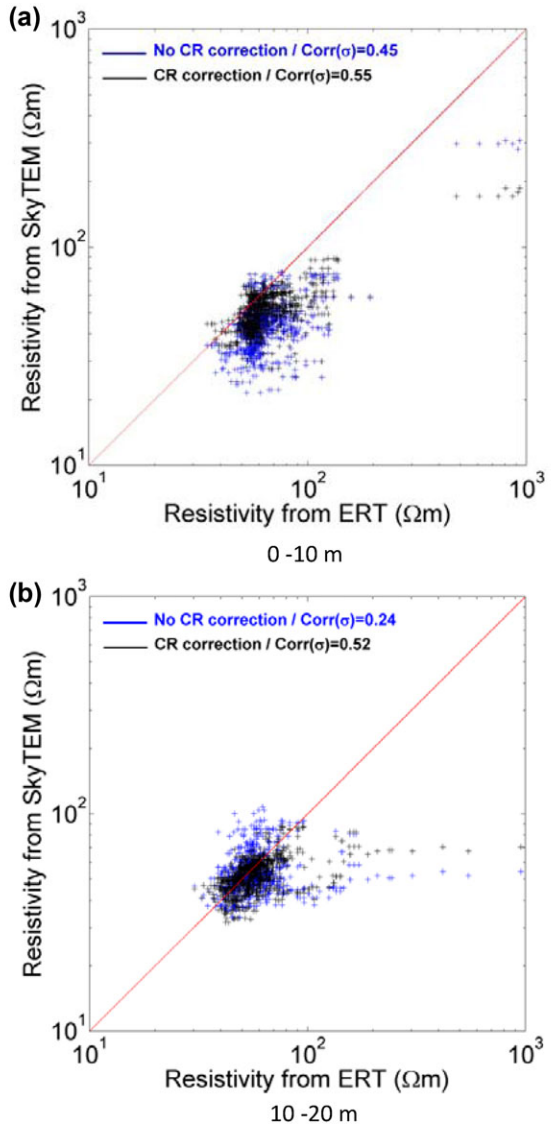

Figure 11 Cross-plots between the mean resistivity determined from SkyTEM and the one from ERT: (a) for the depth interval 0–10 m; (b) for the depth interval 10–20 m. SkyTEM resistivities are taken directly from the closest sounding to the corresponding ERT sounding (<20 m). The red line corresponds to the identity function. Correlation coefficients are computed regarding the conductivity (which is similar to the log of resistivity).

DISCUSSION

To make this coil response removal scheme work for helicopter transient electromagnetic systems we made the following assumptions:

- The secondary field generated by the primary part of the CR is negligible compared to the earth response induced by the rest of the ramp-off. The current producing the CR is less than 0.01 A and therefore the secondary field generated is much lower than the secondary field generated by the rest of the turn-off. The total measured magnetic field at very early times can then be considered as the superposition of the off-time earth response and the CR response and classical off-time modelling can be kept.
- The shape of the CR is stable since it depends only on the capacitance, the inductance and to a very limited degree on the resistance of the transmitter wire (cf. demonstration and field measurements in the second and third parts of the present paper, respectively).

- Since the resistance of the transmitter wire is very low, in the order of a few Ωm, its change with temperature does not have any impact on the CR. Also the variation of the resistance is only about 0.3 ‰ per degree, which gives a variation of 9% for a temperature difference of 30 °C between HA (1000 m) and production altitude (30 m) measurements. This means that temperature compensation does not have to be considered when using the recorded shape of the CR at HA for inverting data acquired closer to the surface.
- The amplitude variation of the CR requires the estimation of a correction factor only, this one being close to 1 thanks to the rigidity of the system. A stable geometry of the system stated at least during each single flight is a key point to obtain accurate modelling of the CR along the flight lines. However, a larger correction factor could be estimated for HTEM systems, which are not as rigid as SkyTEM, since the inversion of this parameter is done in the logarithmic space.

The above mentioned assumptions are valid not only for SkyTEM but for any other HTEM system. In general, there are some remarks and requirements for applying the presented CR correction:

- For systems with a non step-off waveform, i.e., with a relatively slowly decaying waveform, the limitation in the high-frequency content makes CR correction not a crucial processing step for improving the near-surface resolution. The presented CR correction is also not meant for on-time measurements, which require other processing and modelling techniques.
- For historic data, if high-altitude measurements are available, it is possible to extract the CR and to use it if the waveform (i.e., its shape) is sufficiently stable. We proposed an optimal position for the receiver coil so that the CR is as low as possible compared to the earth response. This position is not at the centre but slightly outside of the transmitter loop. Central loop configurations are suffering from a quite large CR, a few μs after the end of the ramp. However, a bucking coil is usually employed for such configurations, which annihilates a large part of the residual primary field or CR. The CR correction scheme presented in this paper has not been tested for such central-loop systems holding a bucking coil. This would require further investigations that are outside the scope of this paper.

CONCLUSION

The Coil Response (CR) results from a small amount of current remaining in the transmitter loop right after the defined turn-off time. In order to improve the near-surface resolution of helicopter transient electromagnetic (HTEM) systems, we developed a new procedure for modelling the CR in the very early times before 10 μs. The methodology is based on the combination of high-altitude measurements of the CR with the estimation of a corresponding levelling factor during the resistivity inversion. The high-altitude measurements show a stable shape of the CR, while changes in amplitude need to be compensated by an estimation of the shift factor to follow the little variations of the fixed geometry of the HTEM system.

Several examples (sounding, section and mean resistivity maps) of a SkyTEM survey showed that the CR affects the inversion results in the upper 30 m and that it closely mimics the resistivities obtained by means of more than 100 km of ERT data. The inclusion of the CR is more critical when the resistivity of the ground is larger and/or when the flight altitude is higher, i.e., when earth response is lower. Since a constant low flight altitude is generally not possible over an entire survey area, the CR correction is mandatory for any survey where early gates are used. In the presented method for a fixed-geometry system, it only requires the estimation of one supplementary parameter to correct for small geometry variations of less than 10 cm of the frame structure.

ACKNOWLEDGEMENTS

We wish to thank Gheorghe Goncear from the Nature Agency, the Ministry of the Environment (Denmark) for permission to use the Sorø data set. GeofysikSamarbejdet, a collaboration between the Nature Agency and Aarhus University also supported the work as well as the NiCA (Nitrate Reduction in a Geologically Heterogeneous Catchment) project (www.nitrat.dk), funded by the Danish Council for Strategic Research under contract no. DSF 09–067260.

REFERENCES

Allard M. 2007. On the Origin of the HTEM Species. *Proceedings of Exploration 07, Fifth Decennial International Conference on Mineral Exploration*, 355–374.

Auken E. and Christiansen A.V. 2004. Layered and laterally constrained 2D inversion of resistivity data. *Geophysics* **69**(3), 752–761.

Auken E., Foged N. and Sørensen K.I. 2010. Approaching 10 microsec (and earlier) with the SkyTEM system. ASEG, 21st International Geophysical Conference and Exhibition, Sydney.

Casas A., Himi M., Diaz Y., Pinto V., Font X. and Tapias J.C. 2008. Assessing aquifer vulnerability to pollutants by electrical resistivity tomography (ERT) at a nitrate vulnerable zone in NE Spain. *Environmental Geology* **54**(3), 515–520.

Christiansen A.V. and Auken E. 2012. A global measure for depth of investigation. *Geophysics* **77**(4), WB171–WB177.

Christiansen A.V., Auken E. and Viezzoli A. 2011. Quantification of modeling errors in airborne TEM caused by inaccurate system description. *Geophysics* **76**(1), F43–F52.

Fitterman D.V. and Anderson W.L. 1987. Effect of transmitter turn-off time on transient soundings. *Geoexploration* **24**, 131–146.

Grower F.W. 1946. *Inductance Calculations*. Dover Publication Inc., New York, p. 60–61.

Kamenetsky F. and Oelsner Chr. 2000. Distortions of EM transients in coincident loops at short time-delays. *Geophysical Prospecting* **48**, 983–993.

Legault J.M., Prikhodko A., Dodds D.J., Macnae J.C. and Oldenborger G.A. 2012. Results of Recent VTEM Helicopter System Development Testing over the Spiritwood Valley Aquifer, Manitoba. SAGEEP, **25**, 1, 36.

Macnae J. and Baron-Hay S. 2010. Reprocessing strategy to obtain quantitative early time data from historic VTEM surveys. ASEG, 21st International Geophysical Conference and Exhibition, Sydney.

Nyboe N.S. and Sørensen K. 2012. Noise reduction in TEM: Presenting a bandwidth- and sensitivity-optimized parallel recording setup and methods for adaptive synchronous detection. *Geophysics* **77**(3), E203–E212`.

Rapport Naturstyrelsen. 2008. Kortlægning af grundvandsbeskyttelse i Sorø – Stenlille området.

Schamper C., Auken E. and Sørensen K.I. 2012. A new processing system for very early time SkyTEM101 Data. ASEG, 23rd International Geophysical Conference and Exhibition, Brisbane.

Siemon B., Christiansen A.V. and Auken E. 2009. A review of helicopter-borne electromagnetic methods for groundwater exploration. *Near Surface Geophysics* **7**, 629–646.

Sørensen K.I. and Auken E. 2004. SkyTEM – A new high-resolution helicopter transient electromagnetic system. *Exploration Geophysics* **35**, 191–199.

Steuer A., Siemon B. and Auken E. 2009. A comparison of helicopter-borne electromagnetics in frequency- and time-domain at the Cuxhaven valley in Northern Germany. *Journal of Applied Geophysics* **67**, 194–205.

Timofeev V.M. and Novikov P.V. 1990. Distortions of the early stage of transients. In: *Electromagnetic Investigations of the Upper Part of the Earth's Crust*, pp. 14–16. Nauka, Moscow (in Russian).

Viezzoli A., Christiansen A.V., Auken E. and Sørensen K.I. 2008. Quasi-3D modeling of airborne TEM data by spatially constrained inversion. *Geophysics* **73**(3), F105–F113.

Ward S.H. and Hohmann G.W. Investigations in geophysics No.3: Electromagnetics methods in applied geophysics (vol. 1, Theory), (ed. M.N. Nabighian), part 4: Electromagnetics theory for geophysical applications.

APPENDIX

Decay of the current in the transmitter loop

If Kirchhoff voltage law is applied to the circuit in Fig. 2(a), one gets the relations:

$$U_{R_w} + U_L - U_C = 0, \tag{A1}$$

$$U_C - U_{R_d} = 0, \tag{A2}$$

which give in terms of resistances and currents in the frequency domain:

$$R_w I_2 + jL\omega I_2 - \frac{1}{jC\omega} I_1 = 0, \tag{A3}$$

$$\frac{1}{jC\omega} I_1 - R_d I_d = 0, \tag{A4}$$

with $j^2 = \sqrt{-1}$.

Or because of the Kirchhoff current law:

$$I = I_d + I_L, \tag{A5}$$

$$I_L = I_1 + I_2, \tag{A6}$$

the current in the damping resistance can be replaced by:

$$I_d = I - (I_1 + I_2). \tag{A7}$$

Then the coupling of equations (A3) and (A4) becomes:

$$R_w I_2 + jL\omega I_2 - \frac{1}{jC\omega} I_1 = 0, \tag{A8}$$

$$R_d I_2 + (\frac{1}{jC\omega} + R_d) I_1 = R_d I, \tag{A9}$$

where the two unknowns are I_1 and I_2. If I_2 is replaced in equation (A9) by its expression in equation (A8), one obtains for $I1$:

$$I_1 = I \frac{jR_d C\omega(R\omega + jL\omega)}{R_d + jR_d C\omega\,(R_w + jL\omega) + R_w + jL\omega}. \tag{A10}$$

The resistance of the wire, R_w, is very low and generally below a few Ω, even for large loops of several hundred square metres. We then make the approximation $R_w \approx 0$. By setting $s = j\omega$, equation (A10) simplifies to:

$$I_1 = I \frac{R_d C L s^2}{R_d\left(1 + CLs^2\right) + sL}. \tag{A11}$$

The roots of the denominator are:

$$s_{1,2} = \frac{-L \pm \sqrt{L^2 - 4R_d^2 LC}}{2R_d LC}. \tag{A12}$$

The critical mode corresponds to the case where $L^2 - 4R_d^2 LC = 0$, i.e., when:

$$R_d = \frac{1}{2}\sqrt{\frac{L}{C}}. \tag{A13}$$

The damping resistor is set to this value so that the shortest possible aperiodic process develops.

Or I_2 can be expressed as:

$$I_2 = I_1 \frac{1}{jC\omega\,(R_w + jL\omega)}, \tag{A14}$$

$$= I_1 \frac{1}{sC\,(R_w + sL)}, \tag{A15}$$

$$\approx I_1 \frac{1}{CLs^2}. \tag{A16}$$

If I_1 is replaced by equation (A11):

$$I_2 = I_1 \frac{R_d}{R_d\left(1 + CLs^2\right) + sL}. \tag{A17}$$

which gives by using the damping resistance value at the critical mode (equation (A13):

$$I_2 = I \frac{1}{(\sqrt{LC}s + 1)^2}. \tag{A18}$$

During a step on or a step-off the injected current is expressed in the time domain as:

$$i(t) = IH(t), \tag{A19}$$

$$i(t) = I(1 - H(t)), \tag{A20}$$

with $H(t)$ the Heaviside function whose spectrum is $1/s$. The spectrum of the current in the transmitter wire during a turn on is then:

$$I_2 = I \frac{1}{s(\sqrt{LC}s + 1)^2}. \tag{A21}$$

Or more compactly:

$$I_2 = I \frac{a^2}{s(s + a)^2}, \tag{A22}$$

with $a = 1/\sqrt{LC}$

The tables of Laplace transforms give the following expression in the time domain:

$$i_2(t) = Ia^2 \times \frac{1}{a^2}[1 - (1 + at)\,\mathrm{e}^{-at}], \tag{A23}$$

$$i_2(t) = I[1 - (1 + at)\,\mathrm{e}^{-at}], \tag{A24}$$

which gives for a turn-off

$$i_2(t) = I\,(1 + at)\,\mathrm{e}^{-at}. \tag{A25}$$